Design of a High-Resolution and High-Sensitivity Scintillation Crystal Array for PET With Nearly Complete Light Collection

Craig S. Levin, *Member, IEEE*

***Abstract*—Spatial resolution improvements in positron emission tomography (PET) can be achieved by developing detector arrays with finer resolution elements. To maintain high sensitivity and image quality, the challenge is to develop a finely pixellated scintillation crystal array with both high detection efficiency and high light collection. High detection efficiency means the crystals must be relatively long and tightly packed. Extracting a high fraction of the available scintillation light from the ends of long and skinny crystals proves to be very difficult and there is a strong variation with light source depth. The result is inadequate energy resolution. To facilitate light collection, the crystals must be highly polished, which significantly increases costs and complexity. In this paper, we examine this poor light collection phenomenon in more detail. We also describe a novel solution we are developing for readout of an array of 1 mm crystals using avalanche photodiodes (APD). We demonstrate through optical photon tracking simulations that the crystal light collection for this new design is nearly perfect ($\geq$95%) and is independent of the crystal length, width, and surface treatment and origin of the light created.**

***Index Terms*—Avalanche photodiodes, high-resolution imaging, light collection, positron emission tomography (PET), scintillation detectors.**

I. Introduction

WE ARE developing an ultra-high resolution scintillation detector array for positron emission tomography (PET). Spatial resolution improvements in PET may be achieved by developing a detector array with finer ($\leq$2 mm wide) resolution elements. However, to realize the desired spatial resolution improvements in reconstructed images, the system sensitivity must also significantly increase to maintain adequate signal-to-noise ratio (SNR) per image resolution element [1]. High resolution is needed for breast and small animal imaging, which are high sensitivity configurations that will help to realize the desired spatial resolution improvements. To maintain high detection sensitivity and good image quality, the challenges are to develop a finely pixellated scintillation crystal array with both high detection efficiency and high light collection. High detection efficiency means the crystals must be relatively long, tightly packed, and cover a relatively large axial field-of-view (FOV).

Unfortunately, extracting a high fraction of the available scintillation light from the ends of long and narrow crystals proves to be very difficult due to a poor aspect ratio for light collection. The result is lower SNR, relatively small pulse heights (reduced sensitivity), and inadequate energy resolution (reduced Compton scatter rejection capabilities). This low light extraction also contributes to nonoptimized coincidence time resolution. To facilitate light collection, the crystal sides must be highly polished, which significantly increases complexity and costs. Furthermore, the light collection efficiency depends upon the origin of the created scintillation light and is worse for points further away from the photodetector. This further degrades energy resolution.

There are several groups developing ultrahigh-resolution PET systems using scintillation crystals (e.g., [2]–[4]). In these designs, either only a fraction of the available scintillation light from 511-keV photon interactions is extracted from the tiny crystals or some sort of compromise between detection efficiency (length), spatial resolution (width), and light collection is made. If optical fibers are used for light readout of crystals, as in the system described in [5], even further light loss occurs. Indeed, assuming perfectly polished $2 \times 2 \times 10$ mm^3 lutetium oxyorthosilicate (LSO) crystals coupled one-to-one to a 2-mm-diameter, 10-cm long optical fiber [5], an additional factor $>$2 drop-in light collection efficiency may be expected and only a very small fraction of the available signal is utilized. Even further, light loss occurs without the one–one crystal-fiber coupling [6].

In this paper, we describe this poor light collection phenomenon in more detail. We also describe a solution to these problems we are developing that uses avalanche photodiodes (APDs) in a novel light readout configuration for long and narrow crystals. We demonstrate through optical photon tracking Monte Carlo simulations of the scintillation light that with this new design the light extraction from 1-mm-wide crystals is nearly perfect ($\geq$95%) and is independent of the length, width, surface treatment of the crystals, and origin of the created light. We present the design of a prototype APD array we are currently testing. Of interest is also the degree of Compton scatter and crystal penetration that occurs in these minute crystals. We studied these effects through simulation and present the results in the next to last section.

Manuscript received December 3, 2001; revised July 22, 2002. This work was supported in part by a grant from the Susan G. Komen Breast Cancer Research Foundation.

The author is with the VA Medical Center and the University of California, San Diego School of Medicine, San Diego, CA 92161 USA (e-mail: clevin@ucsd.edu).

Digital Object Identifier 10.1109/TNS.2002.803870

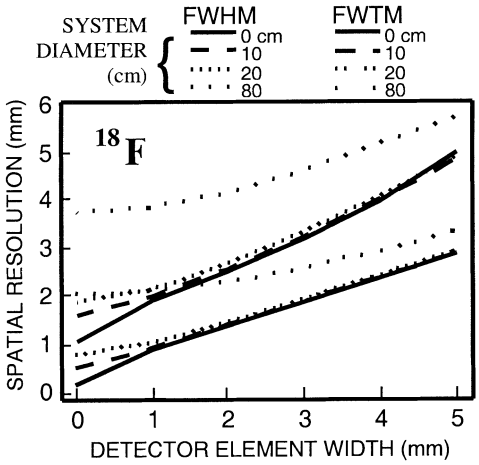

Fig. 1. Calculated point-source spatial resolution [full width at half maximum (FWHM) and full width at tenth maximum (FWTM)] attainable for ^{18}F PET for various system diameters as a function of detector element size. 700-μm FWHM resolution is feasible with 1-mm detector elements and $\leq$20-cm system diameter/detector spacing (adapted from [7]).

II. Theoretical Considerations

A. Spatial Resolution Potential of PET Motivation for 1-mm Detector Pixels

To date, no scintillation crystal-based PET system has achieved the fundamental spatial resolution potential inherent to positron emission imaging. The physical spatial resolution limit is determined by a convolution of three blurring factors: positron range, annihilation photon noncollinearity, and intrinsic detector resolution [7], [8]. Fig. 1 shows a plot of the calculated spatial resolution for ^{18}F determined by these three factors for various system diameters (or, equivalently, detector separations) as a function of detector element size. In principle, submillimeter resolution is attainable with 1-mm detector pixels and $\leq$20-cm detector separation. A gas-filled system [9] has achieved near the spatial resolution potential for PET, but that system has nonoptimal sensitivity and essentially no energy resolving power.

B. Poor Light Collection From Long and Narrow Crystals

The fraction of the available scintillation light that is collected at the end of a crystal, or *light collection efficiency*, in general depends on the *aspect ratio* (ratio of the crystal readout cross-sectional area A, to length L). The aspect ratio affects the degree of light absorption and trapping within the crystal and at the surfaces. A high aspect ratio allows optimal light collection. A low aspect ratio for example would mean that there would be on average more surfaces (and associated losses) that light rays would encounter before collection and potentially more bulk photon absorption.

An upper limit on light collection efficiency f, for a low aspect ratio crystal may be estimated by inspection of Fig. 2 assuming ideal conditions and a poor crystal aspect ratio for light collection. The light loss fraction depends on how much light impinges on the crystal sides at angles less than the critical angle θ_c for total internal reflection and refracts out of the crystal. This

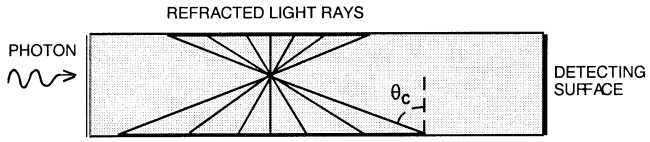

Fig. 2. Depiction of a major mechanism for light loss from poor aspect ratio (long and skinny) crystals. Annihilation photon interaction point is shown near the center; sample light rays emitted from that point are shown. Most of the light impinging on the crystal sides at angles less than the critical angle will exit the crystal or reflect back at similar angles and not be piped down to the small photo-detecting end. Reflectors are on sides and back.

is similar in principle to light transmission into and down a nonclad optical fiber. The solid angle of lost light through one side face Ω_L is approximately given by

$$\Omega_L \approx \pi \tan^2 \theta_c \approx \pi / n^2 \tag{1}$$

where n is the refractive index, θ_c is the critical angle for total internal reflection, and we have used Snell's law and expanded the result to first order in $1/n^2$. An estimate for the lower limit on the total light loss fraction may be obtained by multiplying Ω_L by four and dividing by 4π. Thus, the upper limit estimate of the light collection efficiency f for low aspect ratio crystals is

$$f \approx 1 - 1/n^2 \tag{2}$$

which depends only upon n and not on crystal details.

According to this expression, higher n crystals will on average collect a larger fraction of the available scintillation light. For example, this formula predicts a maximum light collection efficiency of 69% and 78%, respectively, for LSO ($n = 1.82$) and bismuth germanate (BGO) ($n = 2.15$) (although, certainly LSO will yield a larger absolute number of photons). In reality, due to imperfect surfaces, external reflectors, and depth-dependent effects, the precise light collection efficiency in general is strongly dependent on the particular crystal aspect ratio used.

III. Light Collection Simulations

Light collection simulations were performed using DETECT [10] which models and tracks the propagation of light photons through the crystal. For these simulations it was assumed that 511-keV interactions produce 10 000 light photons [11] within a volume of 0.001 mm^3 at several points within an LSO crystal. For each light origin, the simulation was performed three times and averaged to improve accuracy. For poor aspect-ratio crystals, the light collection efficiency strongly depends upon the light origin within the crystal. The average light collection efficiency for a given crystal configuration was obtained by taking a mean of the simulation results for different source depths weighted with the 511-keV photon interaction probability in LSO at any given depth.

Fig. 3 shows the results of Monte Carlo simulations of light collection from the ends of long and narrow scintillation crystals for two different surface conditions. The ideal condition is a perfectly polished crystal with an air gap and a high reflectivity ($R = 0.98$) diffuse reflector on all surfaces except the detecting end. These conditions will promote internal reflection toward

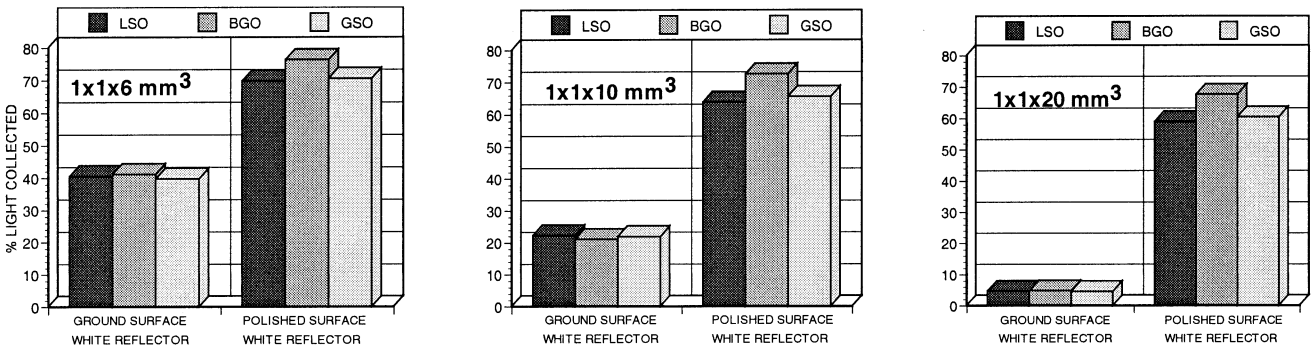

Fig. 3. Average fraction (%) of the available scintillation light collected from the ends of different length and type of 1-mm-wide scintillation crystals for two different crystal surface conditions. Even with the most ideal surface conditions, only a fraction of the available light is collected. In practice, the light collection efficiency lies somewhere between the two extremes represented by the ground and perfectly polished surfaces (e.g., 20%–63% for $1 \times 1 \times 10$ mm^3 LSO).

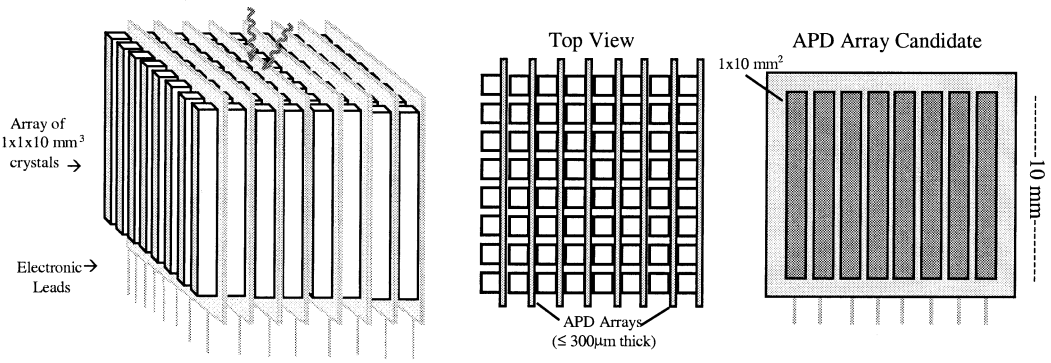

Fig. 4. One proposed readout scheme for an array of $1 \times 1 \times 10$ mm^3 crystals using very thin APD arrays that fit compactly ($\leq$300 μm thick) between each crystal plane. One candidate APD array design is shown. In this example, each APD element may be segmented lengthwise for depth of interaction information. 511-keV photons enter from the top as shown.

the crystal end. The other surface condition is ground (diffuse Lambertian) with the same reflector type. Since in reality it is never possible to achieve surface conditions that promote maximum total internal reflection, under practical experimental conditions the measured light collection efficiency would lie somewhere between the two extremes dictated by the ground and perfectly polished conditions for a given crystal aspect ratio. For example, for a $1 \times 1 \times 10$ mm^3 LSO crystal, light collection efficiency will be somewhere between 20% and 60%, and only a fraction of the available detector signal would be realized.

Note that, as predicted, due to BGO's higher refractive index its polished light collection efficiency is higher than that of the other crystals. Note also that for these simulations we were concerned mainly with the fraction of light exiting the crystal and 0.05 mm of optical coupling compound and entering the photodetector. To determine the average total photoelectron signal created by the photodetector, one would multiply the absolute number of photons collected by the quantum efficiency of the device.

IV. How to Obtain Nearly Perfect Light Collection From Long and Narrow Crystals

Fig. 4 depicts one proposed readout scheme that facilitates nearly perfect light collection. In such a scheme, a one–dimensional (1-D) APD "line" arrays with rectangular pixel elements read out light from the long crystal faces [12]. An alternate design could use the position-sensitive APD (PSAPD) described in [13]. The PSAPD requires only four electronic readout channels to position an input light pulse. Note that the concept we propose exploits the high compactness of semiconductor photodetectors for tightly packed crystal readout schemes that are unavailable to photomultiplier tubes (PMT).

The advantage of collecting the light from the relatively large crystal side faces is that the light crystal aspect ratio (A/L) is significantly increased (10 : 1 versus 1 : 10 for a $1 \times 1 \times 10$ mm^3 crystal). Results for light collection simulations of the configuration depicted in Fig. 4 are presented in Fig. 5. The light collection efficiency is nearly perfect ($\geq$95%), independent of crystal length, width, and surface conditions, and is also independent of the origin of light creation (compare with Fig. 3). This more complete, nonvarying light collection efficiency should lead to more robust detector signals and better energy and perhaps coincident time resolution. The fact that the light collection is independent of surface conditions will also help to significantly reduce crystal array production costs. For example, as long as the crystal faces are flat, freshly saw-cut surfaces may be used.

The main challenges to this scheme are: 1) the APD device thickness must be $\leq$300 μm in between crystal planes to maintain a high crystal packing fraction (low dead area) so not to compromise detection sensitivity and 2) The electronic leads are taken from the bottom of each array as shown. A prototype for the line array shown in Fig. 4 is shown in Fig. 6. Rectangular pixels 0.7×7 mm^2 in area were achieved with a pitch of 1 mm. This array was manufactured using a deep-diffusion

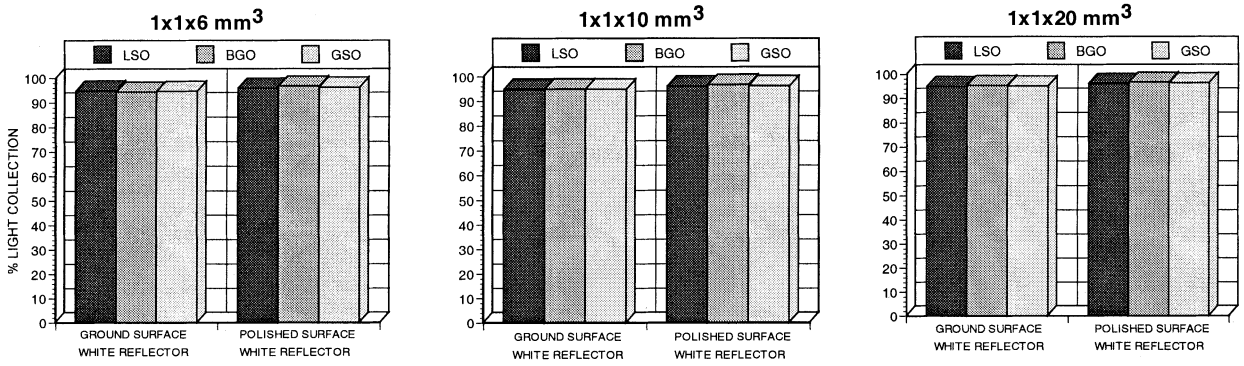

Fig. 5. Nearly perfect ($\geq$95%) light collection efficiency that is independent of crystal length, width, surface conditions, and origin of the scintillation light, is possible with the proposed readout. Compare with Fig. 3 for the conventional readout geometry. The proposed scheme could help to push the limits of PET spatial resolution (see Fig. 1) by allowing high light collection in very fine crystals without compromising detection efficiency (crystal length).

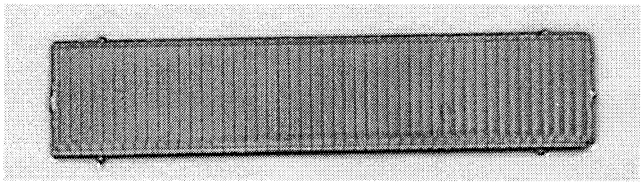

Fig. 6. Prototype APD "line" array has 41 rectangular elements, each 0.7 $\times$ 7 mm^2 in area with a 1-mm pitch. The sensitive area covers $\sim$4 cm in width.

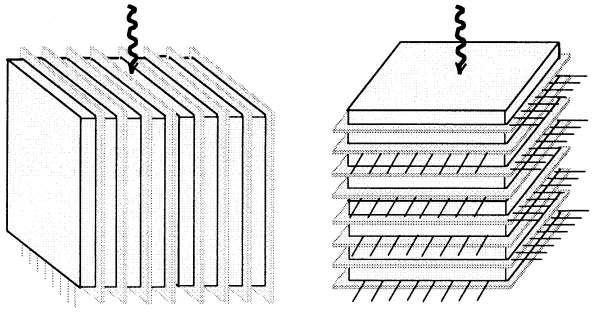

Fig. 7. Alternate detector concepts involving sheets of crystals instead of arrays of minute discrete crystals. The two different configurations are oriented such that the 511-keV photons enter from the top. Both detectors would have interaction depth determination capability. The left design requires very thin photodetectors, while that on the right does not.

process and standard planar silicon device technology [14] and is currently being tested. The capacitance per element of the device is $\sim$3 pF and the typical device gain is $>$200. The current thickness of this particular prototype is $\sim$1 mm. A very thin device may be achieved by significantly reducing the substrate and/or wafer thickness. However, achieving such designs may be challenging since the silicon wafer may not have adequate mechanical support.

A noted advantage of the "edge-on" design depicted in Fig. 4 is that the dead area surrounding the photosensitive area that is common with most semiconductor photodetector array designs does not affect the crystal array packing function (and thus, the sensitivity) as it would in the case of detector arrays that use "face-on" orientation of a photodetector array.

V. APD Dark Noise

Dark noise in APDs comprises parallel and series contributions. The major parallel noise sources arise from the bulk and surface leakage currents of the device. The series component is a function of the device and input preamplifier capacitance. An expression for the rms dark noise for the device, σ_N^2 expressed in terms of the number of electron–hole pairs created is given by [15]:

$$\sigma_N^2 = 2e(I_B \mathrm{F} + I_S/G^2)\tau + 4kTR_S(C_T^2/G^2)1/\tau \quad (3)$$

where e is the electron charge, I_B and I_S are the bulk and surface leakage currents, respectively, F is the APD excess noise factor, G is the device gain, τ the shaping time constant of the amplifier, k is the Boltzmann constant, T the absolute temperature, R_s the preamplifier series resistance, and C_T is the total preamplifier input capacitance from the APD and stray capacitance. One advantage of an APD is that the surface leakage current is not involved in the avalanche process. Since each APD array element is coupled to a crystal side face that is only $\leq$10 mm^2 in area, C_T will be relatively small (the APD capacitance is only $\sim$3 pF in the prototype shown in Fig. 6). If C_T is small and the APD gain G is relatively high ($>$200), from (3) we see that the noise will be relatively low and determined by the bulk leakage current term. For the prototype device, the expected dark noise is on the order of 250 eV (30 e^- rms) per element [14]. As a result, excellent energy and coincident time resolution have been measured with similar APDs [16].

VI. Potential Design Variations

Potential difficulties with tomograph designs comprising many small scintillation crystals are that it is costly and complex to handle many minute crystal elements and align them with their corresponding photodetector element. Any slight misalignment could mean reduced light collection. In addition, fabricating high-performance APD arrays that are $\leq$300 μm as depicted in Fig. 4 may be challenging. In Fig. 7, we show alternate solutions comprising sheets of 1-mm-thick crystals to replace the discrete crystal planes depicted in Fig. 4. Working with sheets of crystals, perhaps 10 $\times$ 10 $\times$ 1 mm^3, instead of arrays of discrete 1 $\times$ 1 $\times$ 10 mm^3 crystals has the advantage that it is significantly easier and less expensive to cut larger

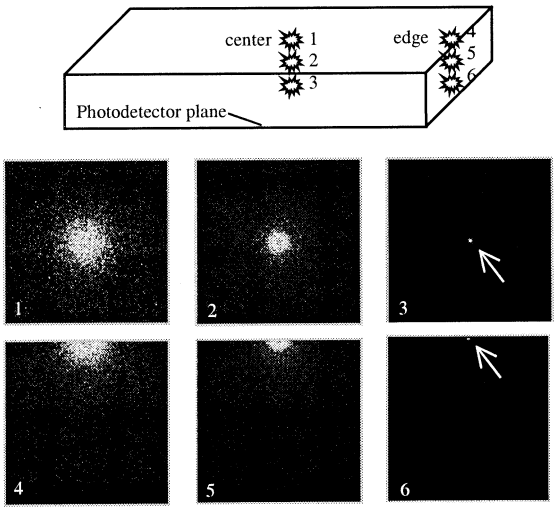

Fig. 8. Top: Configuration for light collection simulations in a $10 \times 10 \times 1$ mm^3 LSO crystal for two x–y point light source locations (center and edge) and three distances z of the light source from the photodetector face (top, middle, bottom). Bottom: Results of simulations show the light distributions seen at the photodetector plane for the six light source locations. Note that for source positions at the detector plane, the light distribution is extremely narrow.

crystal pieces and assemble them into an array. The orientation of the first design (Fig. 7, left) relative to that of incoming photons is the same as for the concept depicted in Fig. 4 and would require $\leq$300-μm APD thickness. Using crystal sheets may ease the difficulties in manufacturing a very thin array since it may be possible to completely remove the array substrate and use the crystal instead as backing for mechanical strength to support the silicon wafer. Either line or square-pixel arrays, or PSAPDs [13] could be used in this design.

The orthogonal configuration (Fig. 7, right) would allow easy depth of interaction determination. This orientation also would allow higher detection sensitivity since incoming photons would not see any crystal gaps due to the array. This orthogonal orientation also has the advantage that a standard thickness APD array could be used. Such a configuration could be developed by using alternate planes of APD line arrays oriented in the x and y directions on either side of each crystal plane in a "cross-grid" type readout. An interaction point in any crystal plane could be determined by which cross-strip x and y elements were hit. This orthogonal orientation could alternately be achieved with a single PSAPD [13] or a more standard square-pixel array in between each crystal plane.

Using crystal sheets instead of minute discrete crystals also has the advantage that the light distribution may involve multiple APD array elements and one may achieve better spatial resolution than the size of the elements by forming an appropriate weighted mean of the various signals involved. A potential disadvantage of this property is that less SNR is available per array element. To study this latter effect, we simulated light collection from the large face of a thin, $10 \times 10 \times 1$ mm^3 LSO crystal sheet. We simulated point sources at the center and edge of the large area as depicted at the top of Fig. 8. For these central and edge locations, we simulated three different source distances with respect to the photodetector plane as shown: *top* position corresponded to $\sim$0.1 mm from the top face, the *middle* position to the crystal center, and *bottom* to $\sim$0.1 mm from the bottom plane where the photodetector is coupled. Note that the total light collection from the large face was nearly perfect independent of crystal surfaces and source position since this is also a very high aspect ratio (100 : 1) for light collection.

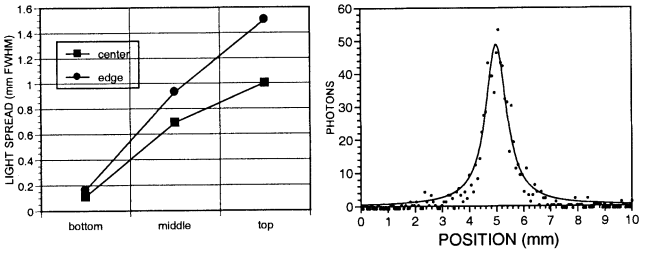

Fig. 9. Left: FWHM of the light distribution profiles created in a $10 \times 10 \times 1$ mm^3 crystal sheet. Right: An example fit of a light spread profile to a Lorentzian distribution.

The simulated light distributions seen at the photodetector plane are shown at the bottom of Fig. 8. Note that for source positions very close to the photodetector plane the exiting light distribution is extremely narrow (see arrows). This is due to the fact that the cone of refracted light ($\theta_i < \theta_c$) subtended from the light origin to the crystal bottom plane and exiting the crystal on first pass, and that light cone which reflects off the top and subsequently exits the bottom surface are narrower for closer distances to the photodetector surface. Thus, the base of the detected light cone will also be narrow. The light rays that undergo total internal reflection ($\theta_i > \theta_c$) will for the most part be trapped within the crystal and not contribute significantly to the tails of the distribution.

Light distribution shapes were quantified by fitting horizontal profiles through the center of the light distributions shown in Fig. 8 to a Lorentzian function

$$f(x) = Aw/[(x - x_0)^2 + (w/2)^2)] \tag{4}$$

where x_0 and w respectively, are the peak location and FWHM of the distribution $f(x)$. The extracted FWHM values and a sample fit (distribution 5 of Fig. 8) are shown in Fig. 9. The results in Fig. 9 indicate that the FWHM of the light spread profiles typically do not extend more than 1 mm laterally, with the broadest spread (1.5-mm FWHM) occurring when the light is created 1 mm (the furthest distance possible) from the photodetector face. In all cases, at least 90% of the light is contained within 3 mm laterally. Assuming 1-mm-wide array pixels (see Figs. 4 and 6), this suggests that only three elements may be necessary to collect a high fraction of the available light created within a crystal sheet. An event could be positioned using a weighted mean on only three signals, avoiding excessive uncorrelated noise propagation, or by selecting the pixel with maximum signal. With a weighted mean approach, resolution would be less than the pixel width.

VII. Annihilation Photon Scatter and Penetration

Using very minute ($1 \times 1 \times 10$ mm^3) array crystals, the question arises whether intercrystal Compton scatter or penetration of 511-keV photons causes severe positioning errors. To study this we used Monte Carlo simulation code [17] to model the photon interactions in the LSO crystals.

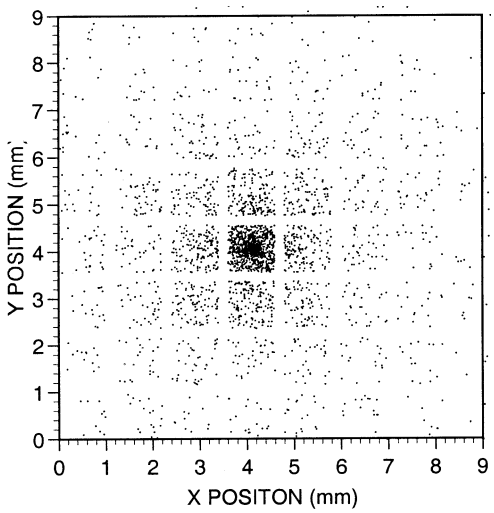

Fig. 10. Distribution of interaction vertices projected onto the x–y plane for photons normally incident on a central $1 \times 1 \times 10$ mm^3 crystal of an 8×8 array.

TABLE I
CALCULATED PROBABILITIES OF VARIOUS TYPES OF 511-keV PHOTON INTERACTIONS IN $1 \times 1 \times 10$ AND $1 \times 1 \times 30$ mm^3 CRYSTAL ARRAYS

1x1x10 mm^3 Crystals	% of Detected Events	% of Total Events	**1x1x30 mm^3 Crystals**	% of Detected Events	% of Total Events
PE Only	61.7	20.0	PE Only	55.8	30.4
CS+PE	37.1	11.9	CS+PE	43.1	23.5
CS Only	1.2	0.4	CS Only	1.0	0.6
No Interaction	-	43.7	No Interaction	-	8.8
E<E$_T$	-	24.0	E<E$_T$	-	36.7
Positioned correctly	**75.3**	**24.3**	**Positioned correctly**	**78.5**	**42.7**

A. Intercrystal Compton Scatter

We simulated a narrow beam of 20 000 annihilation photons hitting normal to the face of one of the central crystals in the 8×8 fine-crystal array depicted in Fig. 4. An event energy threshold (E_T) of 350 keV and a cutoff of 10 keV per interaction were assumed. Up to six interactions per event were allowed, but in reality the number of vertices per event was never greater than three in the simulations. Fig. 10 shows a scatter plot of the photon interaction vertices in the array projected onto the 2-D x–y plane. Table I (left) summarizes the fractions of the different types of interactions that occur [Photoelectric (PE), Compton scatter (CS), and both (CS+PE)] in the $1 \times 1 \times 10$ mm^3 crystal array relative to both the number of detected ($\sim$6400) and total (20 000) simulated events. Coherent scatter effects were included, but contributed insignificantly to the results for the energies of interest. Note that both the number of incoming photons that did not interact and those with total energy deposited less than $E_T = 350$ keV do not count as detected events. Our definition of a correctly positioned event is when the location of maximum energy deposition for that event resides within the crystal being irradiated by the narrow photon beam. Our results predict that 75% of the detected events are binned correctly for photons normally incident on a given crystal and the FWHM of the intrinsic detector response function is not affected by Compton scatter. Mispositioned scatter events contribute to the tails of the response function and represent $\sim$25% of the detected events. These encouraging results are most likely due to the fact that the incoming beam is normal to the central crystal and the photofraction in LSO at 511 keV is substantial ($\sim$32%). Also, many scatter photons escape and/or their total energy deposition is $<$350-keV threshold.

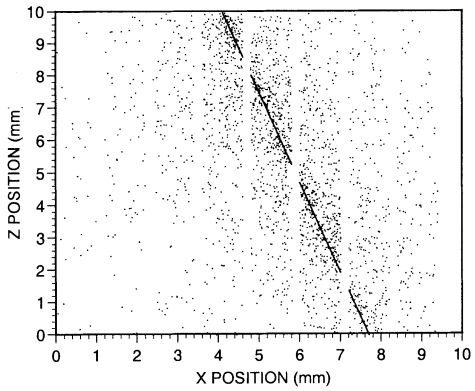

Fig. 11. Interaction vertices in an 8×8, $1 \times 1 \times 10$ mm^3 crystal array projected onto the x–z plane for 20° obliquely incident photons.

For comparison, we also performed the identical simulations for an array of $1 \times 1 \times 30$ mm^3 crystals which we expected to have higher detection efficiency for scatter events. Table I (right) summarizes these results. We see that the overall probability of interaction, including PE and CS+PE, significantly increases with the array of 30-mm-long crystals, while the number of events with energy $<$350 keV increases. However, the breakdown of event types relative to the number of detected events ($\sim$11 000) is similar to that calculated for the 10-mm-long crystals. The fractions of correctly positioned events also significantly increase for the thicker crystal array. Again, the tails of the intrinsic response function are affected by inter-crystal scatter, but not the FWHM.

B. Crystal Penetration

Although the FWHM intrinsic spatial resolution was not affected by intercrystal scatter for irradiation normal to the face of a 1×1 mm^2 crystal, most certainly it will be when the photons enter obliquely into the highly discrete array. Oblique photons will especially play a significant role with the high-sensitivity breast and small animal imaging configurations we are interested in since the detectors are in close proximity to the radiation source. For these close-proximity detector configurations, we estimate that an average incidence angle expected is 20° with respect to the normal to the crystal face. We simulated 20 000 photons incident upon the middle of the same central $1 \times 1 \times 10$ mm^3 crystal (see oblique photon entering array in Fig. 4) at a 20° angle and parallel to the x–z plane, with the other conditions being the same as before. A narrow photon beam directed along a line in the x–z plane represents the worse case for crystal penetration since the photons traverse the narrowest portion of the crystal for that incidence angle. Fig. 11 shows the interaction vertices scatter plot projected onto the x–z plane. Table II summarizes the results.

The simulations predict that there is a significant drop in the detection probability compared to the normal incidence case

TABLE II
SUMMARY OF INTERACTION TYPES AND PROPERTIES FOR SIMULATED OBLIQUE INCIDENCE PHOTONS

1x1x10 mm³ Crystals	% of Detected Events	% of Total Events
PE Only	62.3	16.9
CS+PE	36.9	10.0
CS Only	0.8	0.2
No Interaction	-	51.4
$E<E_T$	-	21.5
Positioned correctly	**15.9**	**4.3**

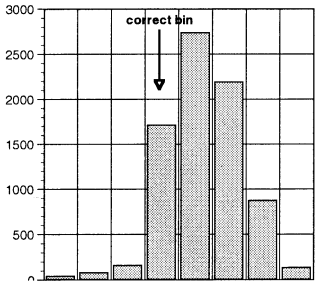

Fig. 12. 1-D histogram of interaction vertices of Fig. 11. Less than 20% of the detected events are positioned in the correct crystal bin.

[Table I (left)] due to more photons escaping. There are, however, more events that are above the 350-keV threshold. Of the detected events (~5400), only 16% are positioned in the correct crystal and the remaining 84% mispositioned events will significantly blur the resolution without interaction depth determination capabilities. The extent of this blurring can be seen from a histogram of the x–z interaction vertices, shown in Fig. 12. Thus, we will need to implement one of the depth resolution schemes we suggested earlier into our design. It is interesting to note that if we turn off Compton scatter in our oblique simulations, the fraction of correctly positioned events increases to ~23%. Thus, it is expected that Compton scatter is the cause of roughly 30% of the mispositioned events for the oblique photon incidence case simulated (the other 70% is due to detector penetration).

VIII. DISCUSSION AND SUMMARY

Submillimeter spatial resolution is feasible for PET using ~1-mm detector pixel elements and close proximity (<20-cm diameter/detector separation), high sensitivity configurations, such as for small animal or breast imaging. The difficulty of developing a finely pixellated scintillation detector array is that typically either light collection or 511-keV detection efficiency are necessarily compromised. Over 10 000 light photons are available from a 511-keV photoabsorption in LSO [11]. High light collection efficiency allows optimal detector signals for high sensitivity. Nearly complete light collection is also desirable for optimal energy resolution and maximum Compton scatter rejection capabilities. Energy resolution and Compton scatter rejection capabilities are already nonoptimal for very narrow crystals since typically light collection depends on the varying interaction points where light is created within the crystal.

Is Compton scatter a problem for imaging small objects such as laboratory animals? Recent data [18] suggest >30% scatter fraction for a three-dimensional (3-D) PET acquisition of a rat-sized object. It is certainly possible to obtain very-high-resolution images with poor or no energy resolution [9], especially using bone imaging tracers, such as $^{18}F^{-}$ that have high target-to-background ratio. However, nonoptimal energy resolution means nonoptimal image contrast and quantitative capability, especially for more diffuse tracer concentrations.

We are developing a detector array solution with a goal of nearly complete light collection from 1-mm detector pixels, independent of light source origin. Simulation results suggest this goal is feasible. These properties facilitate maximum use of the available photons for optimal energy resolution. The design will utilize relatively long crystals and maintain a high packing fraction for high detection efficiency. Simulations show that the crystal surfaces are also unimportant which will help to limit the costs of such a design. The high aspect ratio readout configurations suggested are only available to compact semiconductor photodetector arrays, and not to PMTs.

We are testing a prototype APD line array comprising tiny rectangular pixel elements that will couple one-to-one to the sides of the minute crystals. The fact that the array is 4 cm long would facilitate a relatively large axial sensitivity in one ring of detector modules for a high-resolution small-animal imaging system, or would reduce the number of detector array modules required for a breast imaging system. In principle, arrays of rectangular pixels as wide as 6 cm could be fabricated using standard planar silicon device technology, which would nearly cover the entire length of a mouse.

We are also investigating the use of thin crystal sheets rather than minute discrete crystals to reduce design complexity, and perhaps improve spatial resolution beyond the readout array pixel size. Two new orthogonal configurations were suggested in Fig. 7 with different orientations of the crystal sheets with respect to the incoming photons. Simulation results indicate that there would not be a significant reduction in SNR per pixel element since the light distributions created in these thin sheets are very narrow and extend over only very few photodetector array elements. These new configurations might use segmented APD line arrays or the recently developed position sensitive APDs.

One potential high light collection configuration that we have proposed requires a very thin semiconductor photodetector that fits very compactly between crystal planes (see Figs. 4 and 7, left). With a detector ring comprising 1-mm-thick crystal sheets (Fig. 7, left) separated by 300-μm-thick photodetectors, the transverse linear sampling distance without interleaving would be 1.3 mm, allowing for very high spatial sampling frequencies. Although the crystal packing fraction in this case would only be roughly 70%, with 30% dead space between crystal planes, using crystal dimensions that extend $\geq$2 cm radially, small detector separation (diameter), and wide axial FOV will facilitate very high system sensitivity. We have suggested that a very thin device, perhaps even less than 300 μm, could be achieved by significantly reducing the substrate and/or wafer thickness, and/or by using the scintillation crystal itself for mechanical

support. However, achieving such designs may be challenging since the silicon wafer may not have adequate mechanical support during the fabrication process. These issues will be a subject of future experiments. Note that the alternate design depicted in Fig. 7 (right) does not require a thin photodetector device.

We performed simulations of the effects of intercrystal Compton scatter and penetration on intrinsic resolution. For normally incident photons, the FWHM of the intrinsic response function is unaffected by scatter and over 75% of the detected photons were correctly positioned. Scatter only affects the tails of the response function in this situation. For obliquely incident photons, however, the intrinsic response function is blurred significantly and a majority of the photons are mispositioned. This suggests that for the high-sensitivity imaging configurations proposed, where the detectors are very close to the activity, the interaction depth capabilities that we have proposed are essential. An assessment of positioning accuracy improvements achieved with interaction depth determination capabilities is the subject of future work.

REFERENCES

[1] M. E. Phelps, S. C. Huang, E. J. Hoffman, D. Plummer, and R. Carson, "An analysis of signal amplification using small detectors in positron emission tomography," *J. Comput. Assist. Tomogr.*, vol. 6, pp. 551–565, 1982.

[2] R. S. Miyaoka, S. G. Kohlmyer, and T. K. Lewellen, "Performance characteristics of micro crystal element (MiCE) detectors," *IEEE Trans. Nucl. Sci.*, pt. 2, vol. 48, pp. 1403–1407, Aug. 2001.

[3] Y.-C. Tai, A. F. Chatziioannou, M. Dahlbom, and S. R. Cherry, "System design for a 1 mm^3 resolution animal PET scanner: MicroPET II," in *Proc. 2000 IEEE Nuclear Science Symp. Conf. Rec.*, vol. 3, p. 21/52.

[4] J. Seidel, J. J. Vaquero, I. J. Lee, and M. V. Green, "Experimental estimates of the absolute sensitivity of a small animal PET scanner with depth-of-interaction capability," in *Proc. 2000 IEEE Nuclear Science Symp. Conf. Rec.*, vol. 3, pp. 21/57–59.

[5] S. R. Cherry and Y. Shao *et al.*, "Optical fiber readout of scintillator arrays using a multi-channel PMT: A high resolution PET detector for animal imaging," *IEEE Trans. Nucl. Sci.*, vol. 43, pp. 1932–1937, June 1996.

[6] Y. C. Tai *et al.*, "Performance evaluation of the microPET P4: A PET system dedicated to animal imaging," *Phys. Med. Biol.*, vol. 46, no. 7, pp. 1845–1862, July 2001.

[7] C. S. Levin and E. J. Hoffman, "Calculation of positron range and its effect on the fundamental limit of positron emission tomography system spatial resolution," *Phys. Med. Biol.*, vol. 44, pp. 781–799, 1999.

[8] "Corrigendum for [7]," *Phys. Med. Biol.*, vol. 45, no. 2, p. 559, Feb. 2000.

[9] A. P. Jeavons, R. A. Chandler, and C. A. R. Dettmar, "A 3D HIDAC-PET camera with sub-millimeter resolution for imaging small animals," *IEEE Trans. Nucl. Sci.*, pt. 2, vol. 46, pp. 468–473, June 1999.

[10] G. F. Knoll, T. F. Knoll, and T. M. Henderson, "Light collection in scintillating detector composites for neutron detection," *IEEE Trans. Nucl. Sci.*, pt. 1, vol. 35, pp. 872–875, Feb. 1988.

[11] M. Moszynski *et al.*, "Absolute light output of scintillators," *IEEE Trans. Nucl. Sci.*, vol. 44, pp. 1052–1061, June 1997.

[12] C. S. Levin and E. J. Hoffman, "Investigation of a new readout scheme for high resolution scintillation crystal arrays using photodiodes," *IEEE Trans. Nucl. Sci.*, vol. 44, no. 3, pp. 1208–1213, June 1997.

[13] K. S. Shah, R. Farrel, R. F. Grazioso, and E. Karplus, "APD designs for x-ray and gamma-ray imaging," presented at the 2001 IEEE Nuclear Science Symposium, San Diego, CA, paper #NM-3.

[14] K. S. Shah, R. Farrell, R. Grazioso, and L. Cirignano, "Large area APD's and monolithic APD arrays," in *Proc. 2000 IEEE Nuclear Science Symp. Conf. Rec.*, vol. 1, p. 7/22.

[15] E. Lorenz, S. Natkaniec, D. Renker, and B. Schwartz, , Rep. NIM A344, 1994, pp. 64–69.

[16] Y. Shao *et al.*, "Design studies of a high resolution PET detector using APD arrays," *IEEE Trans. Nucl. Sci.*, pt. 3, vol. 47, pp. 1051–1057, June 2000.

[17] Y. Shao, S. R. Cherry, S. Siegel, and R. W. Silverman, "A study of intercrystal scatter in small scintillator arrays designed for high resolution PET imaging," *IEEE Trans. Nucl. Sci.*, pt. 2, vol. 43, pp. 1938–1944, June 1996.

[18] C. H. Holdsworth, A. Chatziioannou, R. Leahy, Q. Li, C. S. Levin, M. Janecek, M. Dahlbom, and E. J. Hoffman, "Data correction techniques for improving the quantitative accuracy of MicroPET," *J. Nucl. Med.*, vol. 42, May 2001, 201P.